Inorganic Chemistry

Article

pubs.acs.org/IC

d→f Energy Transfer in Ir(III)/Eu(III) Dyads: Use of a Naphthyl Spacer as a Spatial and Energetic "Stepping Stone"

Daniel Sykes, Simon C. Parker, Igor V. Sazanovich, Andrew Stephenson, Julia A. Weinstein,* and Michael D. Ward*

Department of Chemistry, University of Sheffield, Sheffield S3 7HF, U.K.

Supporting Information

ABSTRACT: A series of luminescent complexes based on {Ir(phpy)$_2$} (phpy = cyclometallating anion of 2-phenylpyridine) or {Ir(F$_2$phpy)$_2$} [F$_2$phpy = cyclometallating anion of 2-(2′,4′-difluorophenyl)pyridine] units, with an additional 3-(2-pyridyl)-pyrazole (pypz) ligand, have been prepared; fluorination of the phenylpyridine ligands results in a blue-shift of the usual ^{3}MLCT/^{3}LC luminescence of the Ir unit from 477 to 455 nm. These complexes have pendant from the coordinated pyrazolyl ring an additional chelating 3-(2-pyridyl)-pyrazole unit, separated via a flexible chain containing a naphthalene-1,4-diyl or naphthalene-1,5-diyl spacer. Crystal structures show that the flexibility of the pendant chain allows the naphthyl group to lie close to the Ir core and participate in a π-stacking interaction with a coordinated phpy or F$_2$phpy ligand. Luminescence spectra show that, whereas the {Ir(phpy)$_2$(pypz)} complexes show typical Ir-based emission—albeit with lengthened lifetimes because of interaction with the stacked naphthyl group—the {Ir(F$_2$phpy)$_2$(pypz)} complexes are nearly quenched. This is because the higher energy of the Ir-based ^{3}MLCT/^{3}LC excited state can now be quenched by the adjacent naphthyl group to form a long-lived naphthyl-centered triplet (^{3}nap) state which is detectable by transient absorption. Coordination of an {Eu(hfac)$_3$} unit (hfac = 1,1,1,5,5,5-hexafluoro-pentane-2,4-dionate) to the pendant pypz binding site affords Ir−naphthyl−Eu triads. For the triads containing a {Ir(phpy)$_2$} core, the unavailability of the ^{3}nap state (not populated by the Ir-based excited state which is too low in energy) means that direct Ir→Eu energy-transfer occurs in the same way as in other flexible Ir/Eu complexes. However for the triads based on the{Ir(F$_2$phpy)$_2$} core, the initial Ir→^{3}nap energy-transfer step is followed by a second, slower, ^{3}nap→Eu energy-transfer step: transient absorption measurements clearly show the ^{3}nap state being sensitized by the Ir center (synchronous Ir-based decay and ^{3}nap rise-time) and then transferring its energy to the Eu center (synchronous ^{3}nap decay and Eu-based emission rise time). Thus the ^{3}nap state, which is energetically intermediate in the {Ir(F$_2$phpy)$_2$}−naphthyl−Eu systems, can act as a "stepping stone" for two-step d→f energy-transfer.

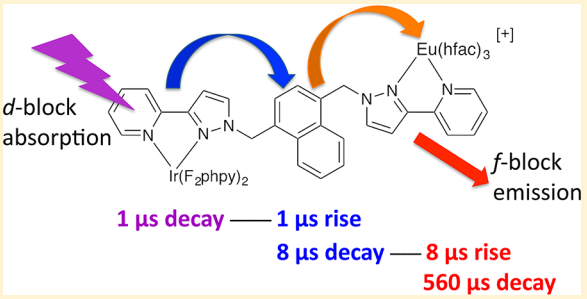

INTRODUCTION

Sensitization of lanthanide luminescence by energy-transfer from a strongly absorbing antenna group is a widely used route to populate the f-f states which are difficult to populate by direct excitation as the transitions are Laporte-forbidden. There has been much recent effort in studying the photophysical properties of d/f dyads in which this antenna group is a transition-metal complex fragment rather than an organic ligand.[1−3] This requires the d-block component to have a high absorption coefficient, and an excited state which is long-lived enough such that energy-transfer to the lanthanide(III) ion is a significant deactivation pathway that competes favorably with other radiative and nonradiative deactivation processes. It also requires that the energy of the excited state of the d-block component lies sufficiently far above that of the emissive level of the lanthanide(III) ion that d→f energy-transfer has a large enough thermodynamic gradient to prevent back energy-transfer.[1a]

Potential applications of such d/f complexes are significant. An appropriate balance between emission colors of different components in the dyads can generate white light from a single molecule, as shown in some Ir(III)/Eu(III) systems which combine blue Ir(III)-based emission and red Eu(III)-based emission.[2e,3e] Given the wide interest in long-lived visible-region luminescence for cellular imaging, molecules combining two luminescent outputs at different wavelengths and on different time scales (d-block, ns to μs timscale; f-block, ms time scale) are of interest as potential new imaging agents.[2f] Lanthanide-based emission can be used for imaging in both the visible region [e.g., Eu(III)] because of its intensity, narrowness, and long lifetimes, and in the near-IR regions [e.g., Yb(III), Nd(III)] because long-wavelength emission can penetrate biological tissue particularly well.[4]

As part of this work it is essential to understand the mechanisms by which d→f energy-transfer occurs.[1b] We have shown in many cases that Förster-type energy-transfer is not feasible over the distances involved between the metal centers

Received: June 4, 2013
Published: September 5, 2013

   dx.doi.org/10.1021/ic401410g | Inorg. Chem. 2013, 52, 10500−10511

because the very low extinction coefficients of the f-f absorptions on the lanthanide ion, which act as the energy-acceptor levels, result in very small donor/acceptor overlap integrals and short critical transfer distances.[2b,e] In contrast, Dexter-type (electron-exchange mediated) energy-transfer can occur because the low intensity of the f-f absorptions is no longer a component of the calculation of the donor/acceptor overlap integral, and conjugated bridging ligands can provide the necessary electronic coupling to facilitate the process.[2b,e] In some other cases, photoinduced *electron*-transfer to generate a charge-separated state is the initial step after excitation,[2g] and collapse of this can provide sufficient energy to sensitize luminescence from the lanthanide [Yb(III)] if the luminescence is in the near-IR region. The issue of how excitation energy is transferred from the d-block antenna to the lanthanide(III)-based emitter is accordingly nontrivial and has numerous subtleties.[1b]

In this paper we describe a new variant of the d→f energy-transfer theme, which is the intermediacy of an organic triplet state on a naphthyl group (hereafter abbreviated as ^{3}nap) that lies spatially and energetically between an Ir(III) unit (energy-donor) and a Eu(III) unit (energy-acceptor). The complexes concerned (Chart 1) are Ir(III)-naphthyl-Eu(III) systems,

Chart 1

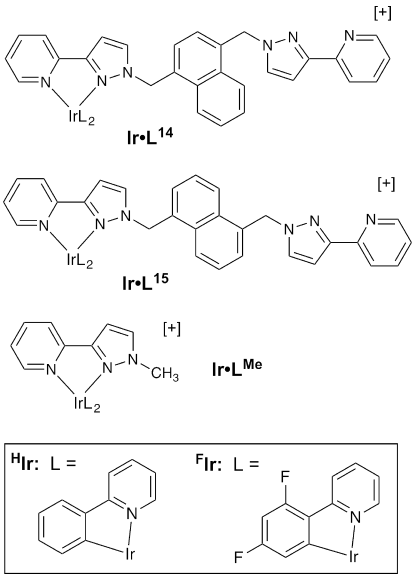

similar in principle to Ir(III)/Eu(III) dyads that we have studied before[2e] but with the added participation of a photophysically noninnocent naphthyl spacer in the bridging ligand. We show how, in cases where the naphthyl triplet state lies significantly below the energy of the Ir(III)-based ^{3}MLCT/^{3}LC state (hereafter abbreviated as ^{3}Ir), it provides a stepping-stone for a two-step energy-transfer process (Ir→naphthyl and naphthyl→Eu). In contrast, with a lower-energy Ir-based energy donor that lies slightly below the energy of the ^{3}nap state, Ir→Eu energy-transfer occurs in a single step without the active participation of a separate ^{3}nap intermediate level, although the naphthyl unit can provide a conduit for mediating the superexchange processes necessary for Dexter-type energy-transfer.

Such behavior has been demonstrated before in several examples of transition-metal based Ru(II)/Os(II) dyads which show long-range energy-transfer between metal complex termini facilitated by triplet states of bridging ligand fragments which are both spatially and energetically intermediate.[5] The current contribution provides an unusual example of such behavior facilitating energy-transfer in d/f systems, and to the best of our knowledge, this is the first demonstration of d-f energy transfer by such a stepwise method. Given the current interest in dual-emissive d/f complexes for applications from display devices to cellular imaging as described above,[1−3] understanding the energy-transfer process which controls their luminescence behavior is of considerable importance.

RESULTS AND DISCUSSION

1. Synthesis and Structural Characterization of Iridium Complexes. The Ir complexes used as the basis of the Ir/Eu dinuclear systems (Chart 1) are all based on bridging ligands which have two bidentate chelating pyrazolyl-pyridine termini.[2d,e] These have several advantages for our purposes. First, when coordinated to Ir(III)/ phenylpyridine units, the resulting complexes have high-energy luminescence in the blue or blue/green region from a mixed ^{3}MLCT/^{3}LC excited state,[6] which has sufficient energy content to sensitize the emissive $^5D_0$ state of Eu(III). Second, attachment of a Eu(hfac)$_3$ unit (hfac = 1,1,1,5,5,5-hexafluoro-pentane-2,4-dionate) to the second NN-chelating site to complete the syntheses of the Ir(III)/Eu(III) dyads is trivial, and occurs in noncompeting organic solvents such as CH_2Cl_2 rapidly according to the equilibrium in Scheme 1.[1,2b−f] Third, syntheses of these

Scheme 1

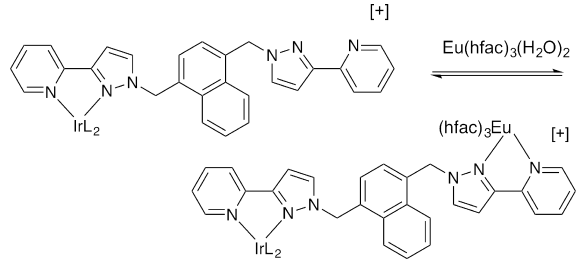

bridging ligands are simple, and a wide range of intermediate organic fragments separating the two pyrazolyl-pyridine termini can be used.[7]

The general synthetic methods used for syntheses of complexes of this type have been described before and do not need repeating.[2d,e] The significant difference for this work is that the bridging ligands all contain naphthyl units rather than phenyl units: in this work we have used the 1,4- and 1,5-disubstituted naphthyl spacer groups to give the ligands L^{14} and L^{15} which we have reported before.[8] These ligands have been used to make the mononuclear Ir(III) complexes [Ir(phpy)$_2$(L^n)](NO$_3$) (n = 14, 15; based on unsubstituted 2-phenylpyridine) and [Ir(F$_2$phpy)$_2$(L^n)](NO$_3$) [n = 14, 15; based on 2-(2′,4′-difluorophenyl)pyridine] which have been satisfactorily characterized by standard methods. For simplicity we abbreviate these complexes as ^{H}**Ir•L**^{14} and so forth for the former series, and ^{F}**Ir•L**^{14} and so forth for the latter series (see Chart 1), where the superscripts "H" and "F" denote the substituents on the phenylpyridine ligands. We have also used for comparison purposed the simple mononuclear complexes ^{H}**Ir•L**^{Me} and ^{F}**Ir•L**^{Me} (Chart 1) which contain no pendant naphthyl groups but just a methyl substituent at the pyrazolyl N^3 position.

dx.doi.org/10.1021/ic401410g | Inorg. Chem. 2013, 52, 10500−10511

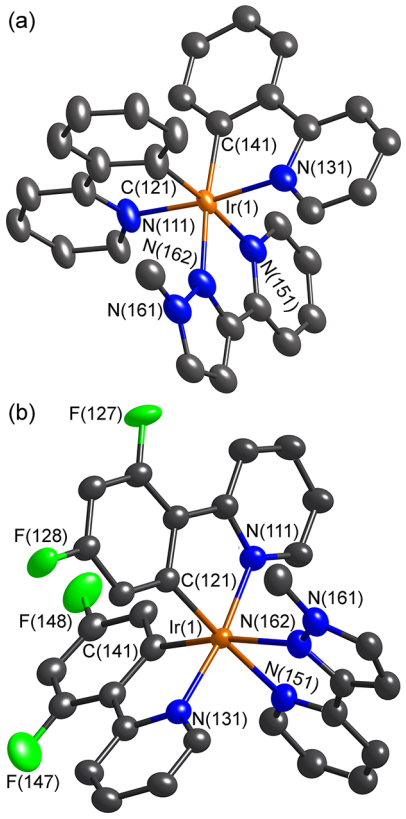

Figure 1. Molecular structures of the complex cations of (a) ^{H}**Ir•L^{Me}** and (b) ^{F}**Ir•L^{Me}**; nitrate anions, solvent molecules, and H atoms are omitted for clarity. Displacement ellipsoids are drawn at the 30% probability level.

Figure 1 shows the crystal structures of ^{H}**Ir•L^{Me}** and ^{F}**Ir•L^{Me}**; crystallographic data are summarized in Table 1, and coordination-sphere bond distances and angles in Table 2. The pseudo-octahedral geometry in each case is unremarkable with the usual *trans, cis*–N_2C_2 arrangement of the two phenylpyridine ligands, which means that the chelating pyrazolylpyridine ligand occupies the coordinates sites *trans* to the two cyclometallating phenyl rings. This arrangement of ligands is shown by all of the other structurally characterized complexes in this paper.

Table 2. Selected Coordination-Sphere Bond Distances (Å) for the New Complexes

^{H}**Ir•L^{Me}**			
Ir(1)–N(111)	2.033(3)	Ir(1)–C(121)	2.035(3)
Ir(1)–N(131)	2.065(3)	Ir(1)–N(162)	2.076(7)
Ir(1)–N(151)	2.079(3)	Ir(1)–C(141)	2.085(3)
^{F}**Ir•L^{Me}•CH_2Cl_2**			
Ir(1)–C(121)	2.007(6)	Ir(1)–C(141)	2.021(6)
Ir(1)–N(131)	2.042(5)	Ir(1)–N(111)	2.047(5)
Ir(1)–N(162)	2.152(6)	Ir(1)–N(151)	2.155(6)
^{H}**Ir•L^{14}•CH_2Cl_2**			
Ir(1)–C(321)	2.012(8)	Ir(1)–C(221)	2.024(8)
Ir(1)–N(211)	2.033(7)	Ir(1)–N(311)	2.038(7)
Ir(1)–N(122)	2.165(7)	Ir(1)–N(111)	2.169(6)
^{F}**Ir•L^{14}•3CH_2Cl_2**			
Ir(1)–C(321)	1.971(11)	Ir(1)–C(221)	2.009(10)
Ir(1)–N(311)	2.045(9)	Ir(1)–N(211)	2.059(8)
Ir(1)–N(122)	2.169(8)	Ir(1)–N(111)	2.169(7)
^{F}**Ir•L^{15}•2CH_2Cl_2**			
Ir(1)–C(321)	2.004(3)	Ir(1)–C(221)	2.009(3)
Ir(1)–N(211)	2.046(2)	Ir(1)–N(311)	2.049(2)
Ir(1)–N(111)	2.153(2)	Ir(1)–N(122)	2.158(2)

The crystal structures of complexes ^{F}**Ir•L^{14}** and ^{F}**Ir•L^{15}** are shown in Figure 2 and have the same basic core structure as shown in the previous example. A notable feature of both structures however is the disposition of the pendant naphthyl group, which lies in each case such that it is stacked with one of the F_2phpy ligands with a separation of about 3.4 Å between the parallel, overlapping aromatic ligand sections. Figure 2c shows an alternative view of ^{F}**Ir•L^{14}** emphasizing the region of overlap between the naphthyl unit and a F_2phpy ligand. This stacking has important potential consequences for the photophysical properties of the complexes as we will see later. Figure 3 shows the structure of nonfluorinated ^{H}**Ir•L^{14}** which shows exactly similar stacking of the pendant naphthyl group with one

Table 1. Crystal Parameters, Data Collection, and Refinement Details for the Structures in This Paper

complex	^{F}**Ir•L^{Me}•CH_2Cl_2**	^{H}**Ir•L^{Me}**	^{F}**Ir•L^{15}•2CH_2Cl_2**	^{F}**Ir•L^{14}•3CH_2Cl_2**	^{H}**Ir•L^{14}•CH_2Cl_2**
formula	$C_{32}H_{23}Cl_2F_4IrN_6O_3$	$C_{31}H_{25}IrN_6O_3$	$C_{52}H_{38}Cl_4F_4IrN_9O_3$	$C_{53}H_{40}Cl_6F_4IrN_9O_3$	$C_{51}H_{40}Cl_2IrN_9O_3$
molecular weight	878.66	721.77	1246.91	1331.84	1090.02
T, K	100(2)	100(2)	150(2)	150(2)	100(2)
crystal system	triclinic	triclinic	monoclinic	orthorhombic	orthorhombic
space group	$P\bar{1}$	$P\bar{1}$	$P2_1/c$	$P2_12_12_1$	$P2_12_12_1$
a, Å	9.7480(6)	9.7883(3)	11.6412(3)	12.7674(5)	12.3327(4)
b, Å	12.7477(8)	12.3108(4)	37.0240(11)	12.8208(5)	12.7350(4)
c, Å	14.4900(9)	13.7024(5)	11.0781(3)	31.9764(15)	31.5659(9)
α, deg	88.000(3)	74.687(2)	90	90	90
β, deg	70.511(3)	89.878(2)	90.0004(12)	90	90
γ, deg	69.778(3)	75.567(2)	90	90	90
V, Å^3	1586.21(17)	1538.69(9)	4774.7(2)	5234.2(4)	4957.6(3)
Z	2	2	4	4	4
ρ, g cm^{-3}	1.840	1.558	1.735	1.690	1.460
crystal size, mm^3	0.35 × 0.35 × 0.3	0.20 × 0.15 × 0.06	0.33 × 0.25 × 0.09	0.41 × 0.23 × 0.22	0.22 × 0.12 × 0.05
μ, mm^{-1}	4.446	4.379	3.092	2.926	2.851
data, restraints, parameters	7199, 359, 428	5239, 332, 257	10949, 5, 657	12001, 19, 655	11548, 2, 580
final *R*1, *wR*2[a]	0.0399, 0.1160	0.0685, 0.2075	0.0273, 0.0544	0.0606, 0.1407	0.0553, 0.1361

dx.doi.org/10.1021/ic401410g | *Inorg. Chem.* 2013, 52, 10500–10511

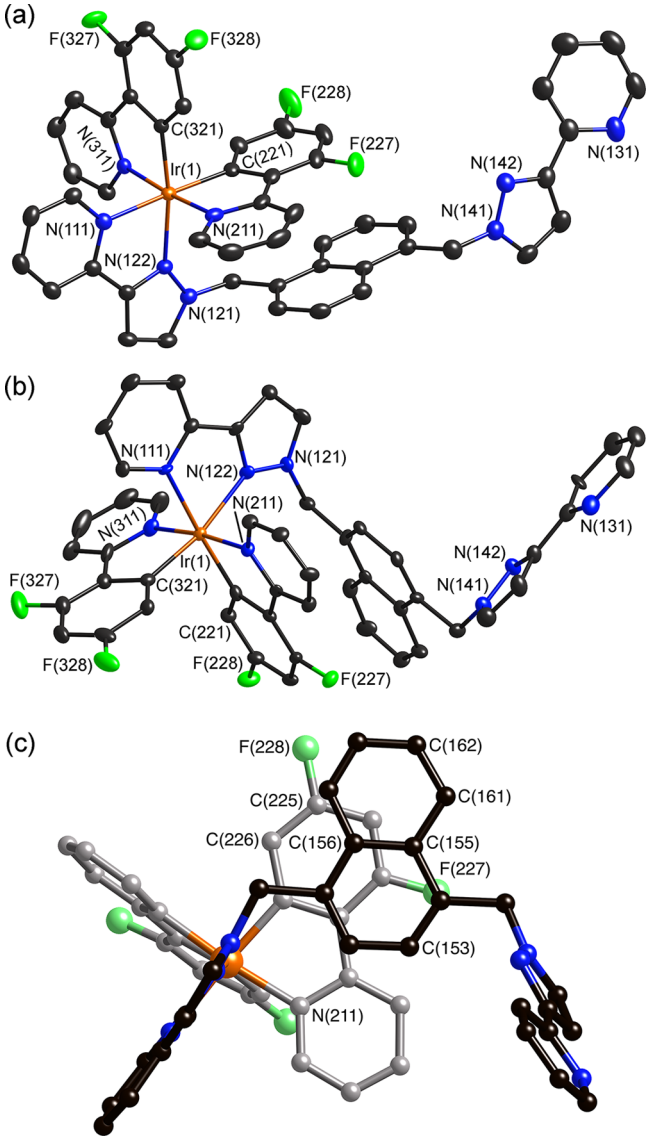

Figure 2. Molecular structures of the complex cations of (a) ^{F}**Ir•L**^{15} and (b) ^{F}**Ir•L**^{14}; nitrate anions, solvent molecules, and H atoms are omitted for clarity. Displacement ellipsoids are drawn at the 30% probability level. Part (c) shows an alternative view of the structure of ^{F}**Ir•L**^{14} emphasizing the aromatic stacking interaction between the pendant naphthyl group (dark gray) and one of the coordinated phenylpyridine ligands (pale gray).

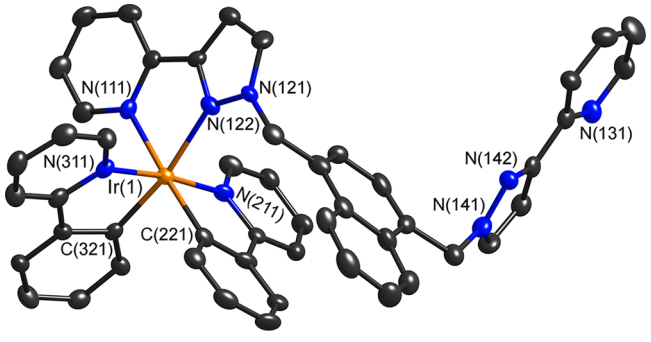

Figure 3. Molecular structure of the complex cation of ^{H}**Ir•L**^{14}; nitrate anions, solvent molecules, and H atoms are omitted for clarity. Displacement ellipsoids are drawn at the 30% probability level.

of the phenylpyridine ligands; note the similarity between the structures shown in Figure 3 and Figure 2b.

2. Photophysical Properties of Ir/Naphthyl Complexes. UV/vis absorption spectroscopic data are summarized in Table 3.

Table 3. Summary of UV/Vis Absorption Spectra for the Complexes in CH_2Cl_2 Solution at Room Temperature

complex	λ_{max}, nm (10^{-3} ε, M^{-1} cm^{-1})
^{F}**Ir•L**^{14}	247 (61), 279 (47), 318 (17), 360 (5.9)
^{F}**Ir•L**^{15}	252 (58), 279 (45), 315 (18), 360 (5.5)
^{H}**Ir•L**^{14}	257 (65), 269 (62), 289 (49), 382 (5.5)
^{H}**Ir•L**^{15}	255 (62), 271 (58), 365 (41), 390 (5.1)
^{F}**Ir•L**^{Me}	256 (44), 291 (27), 341 (17), 362 (6.3), 388 (3.6)
^{H}**Ir•L**^{Me}	256 (44), 268 (41), 287 (29), 340 (9.1), 382 (5.4)

The complexes all show the usual ligand-centered $\pi-\pi^*$ transitions in the UV region, and lower-energy and less intense metal-to-ligand charge-transfer (MLCT) transitions in the region 350−400 nm.

2.1. Emission Spectroscopy of Ir/Naphthyl Complexes. Emission spectra of the mononuclear model complexes ^{H}**Ir•L**^{Me} and ^{F}**Ir•L**^{Me}, which illustrate the emission behavior expected for these metal chromophores, are shown in Figure 4.

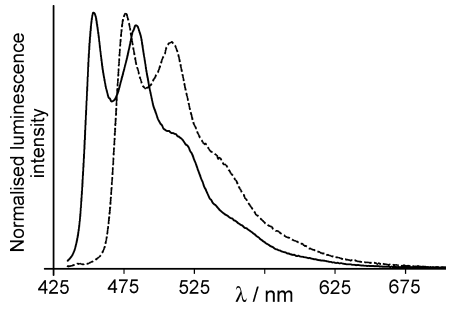

Figure 4. Luminescence spectra (CH_2Cl_2, RT) of ^{H}**Ir•L**^{Me} (dashed line) and ^{F}**Ir•L**^{Me} (solid line).

These spectra are characteristic of the core Ir(III) unit with two *N,C*-donor phenylpyridine ligands and a pyrazolyl-pyridine chelate as we reported earlier,[2d,e] with fluorination of the phenylpyridine ligands in the latter case resulting in a blue shift of the main emission maximum from 476 to 453 nm, a shift of approximately 1100 cm^{-1}.

The nonfluorinated, naphthyl-appended complexes ^{H}**Ir•L**^{14} and ^{H}**Ir•L**^{15} show emission spectra very similar to that of ^{H}**Ir•L**^{Me} with a structured emission whose maximum energy and maximum intensity component is at 477 nm. The luminescence lifetimes in air-equilibrated CH_2Cl_2 are 670 and 690 ns respectively with Φ = 0.31 in each case. These luminescence lifetimes are considerably longer than in the model complex bearing a methyl substituent on the pyrazolyl ring ^{H}**Ir•L**^{Me} (τ = 180 ns, this work) or in a complex with a pendant phenyl group in the same position (τ = 198 ns, previous work).[2e] The presence in ^{H}**Ir•L**^{14} and ^{H}**Ir•L**^{15} of the naphthyl group pendant from the pyrazolyl unit, which lies stacked with one of the phenylpyridine ligands, therefore increases significantly the ^{3}Ir-based emission intensity and lifetime. This most likely indicates operation of the well-known "reservoir effect" arising from the fact that the ^{3}Ir and ^{3}nap excited states are very similar in energy.[9] Notwithstanding this, the emission clearly originates

dx.doi.org/10.1021/ic401410g | *Inorg. Chem.* 2013, 52, 10500−10511

from the ^{3}Ir-based unit in each case as shown by the appearance of the emission spectra, and is not quenched by the naphthyl pendant unit whose lowest excited state is too high in energy to quench the ^{3}Ir-based emission.

In contrast the complexes ^{F}**Ir**•**L**^{14} and ^{F}**Ir**•**L**^{15} show higher-energy luminescence with spectra qualitatively similar to that of ^{F}**Ir**•**L**^{Me} (Figure 4, solid line) with the highest energy emission component at 455 nm, as expected because of the F-atom substituents on the phenylpyridine ligands.[6a] However, the luminescence is—unexpectedly—very weak with quantum yield values of just 0.016 in each case. This is an order of magnitude reduction in emission intensity compared to other complexes of the ^{F}**Ir**•**L** series which do not have naphthyl substituents pendant from the pyrazole ring. For example previously reported analogues in which the naphthyl pendant is simply replaced by a phenyl ring have emission at exactly the same wavelength but with ϕ = 0.13.[2e]

We ascribe the difference in behavior between these two pairs of complexes to the different energetic ordering of the ^{3}Ir and ^{3}nap excited states. The triplet excited state (^{3}Ir) in ^{F}**Ir**•**L** complexes has energy of 22,200 cm^{-1} whereas the energy of the ^{3}Ir state in the nonfluorinated ^{H}**Ir**•**L** complexes is 21,400 cm^{-1} (determined in both cases from the highest-energy component in the 77 K emission spectra).[2d,e] These values may be compared to the energy of the triplet excited state of 21,200 cm^{-1} for free naphthalene[10] which is approximately the same as the excited state energy of nonfluorinated ^{H}**Ir**•**L** complexes (as required for the reservoir effect that we observed, increasing the emission lifetimes),[9] but significantly below the excited state energy of the fluorinated ^{F}**Ir**•**L** complexes. In ^{H}**Ir**•**L**^{14} and ^{H}**Ir**•**L**^{15}, therefore, the ^{3}nap state is unable to quench the ^{3}Ir state of the ^{H}**Ir** unit; but in ^{F}**Ir**•**L**^{14} and ^{F}**Ir**•**L**^{15} the ^{3}nap state acts as a quencher of the higher-energy ^{3}Ir state following ^{F}**Ir**→nap energy-transfer, a process which will be facilitated by the π-stacking that brings chromophore and quencher units into close proximity (see the crystal structures in Figures 2, 3). In principle the sensitized ^{3}nap state could be phosphorescent. In practice however such phosphorescence is not normally detected in fluid solution at room temperature because collision-induced deactivation is many orders of magnitude faster than the radiative decay constant for phosphorescence, and we could detect no ^{3}nap phosphorescence in either air-equilibrated or degassed CH_2Cl_2.

Time-resolved emission measurements on ^{F}**Ir**•**L**^{14} and ^{F}**Ir**•**L**^{15} reveal in each case a quite long-lived decay component of about 500 ns; this may be compared with a luminescence lifetime of 600 ns for the unquenched control complex ^{F}**Ir**•**L**^{Me} under the same conditions. This ≈500 ns emission is however of very low intensity. This is consistent with a mixture of conformers being present in solution. A dominant folded conformer, in which the naphthyl group remains closely associated with the ^{F}**Ir** core because of the π-stacking seen in the crystal structures, must show *complete* quenching of Ir-based luminescence (based on the limitations of equipment) as no short-lived ^{3}Ir-based decay is detectable. A small proportion of a more extended conformer, in which the naphthyl group is remote from the ^{F}**Ir** core and does not quench the ^{3}Ir emission, shows longer-lived Ir-based emission similar to that of ^{F}**Ir**•**L**^{Me}. We note that complex decay kinetics are a common feature of conformationally flexible complexes of this type.[2e,9]

2.2. Transient Absorption Spectroscopy of Ir/Naphthyl Complexes. The complexes have been studied further using transient absorption (TA) spectroscopy to obtain more insight about the localization and kinetic behavior of their excited states. A problem that became quickly apparent is that the ^{3}Ir excited state of the ^{F}**Ir** unit, and the ^{3}nap excited state, give overlapping excited-state absorption spectra. The TA spectrum of the model complex ^{F}**Ir**•**L**^{Me}, on excitation at 355 nm in degassed CH_2Cl_2, shows a broad region of excited-state absorption across the visible region with a maximum at about 420 nm. Coincidentally it is also known that the most intense feature of the TA spectrum of ^{3}nap is at 420 nm,[11] which means that appearance of excited-state absorption in this region is not unambiguously diagnostic of either the ^{3}Ir or the ^{3}nap excited state. However time-resolved measurements allow those to be distinguished, as we will see later, because triplet states of aromatic hydrocarbon groups are much longer-lived than those of heavy metal complexes.

The kinetic behavior of the excited state decay of the mononuclear Ir complexes, as measured by decay of the TA spectrum, is surprisingly complex. This is partly because of the possibility of a mixture of conformers for the complexes ^{H}**Ir**•**L**^{n} and ^{F}**Ir**•**L**^{n} (n = 14, 15) in which the pendant naphthyl groups may be close to, or remote from, the Ir core. In addition the relatively high concentrations used for TA measurements lead to aggregation effects. The resultant decays are multi-exponential but can be *approximately* fitted by two exponential components which indicate the excited state lifetime range in the ensemble (Table 4); correlation between these means that the two components can vary together without making much difference to the quality of the fit. These lifetime values therefore should not be overinterpreted, but taken as an indication of the range of the excited state lifetimes in this system.

For the simple model complex ^{F}**Ir**•**L**^{Me}, the excited-state absorption shows biexponential decay kinetics with lifetimes of $\tau \approx$ 1.7 and 2.6 μs in degassed CH_2Cl_2 (cf. single-exponential decay of 600 ns for luminescence in air-equilibrated CH_2Cl_2 at lower concentration). Longer luminescence lifetimes from a triplet state in the absence of O_2 are to be expected, but we see here the effects of aggregation arising from the higher concentrations used for TA spectra. In agreement with this, time-resolved luminescence measurements on the same solution used for the TA measurements could also be fitted to two lifetime components in the same range (Table 4), in good agreement with the TA spectrum. The important point is that the excited-state absorption at 420 nm therefore arises from the same excited state as does the luminescence, that is, the usual Ir-centered ^{3}(MLCT/LC) state,[6a] and indeed we have seen similar TA spectra for related complexes in previous work.[2e] For the analogous nonfluorinated model complex ^{H}**Ir**•**L**^{Me} the *apparent* maximum in the TA spectrum is at 450 nm (Figure 5b), indicative of a slightly lower-energy T_1−T_2 energy gap compared to ^{F}**Ir**•**L**^{Me}. Again this is not a true maximum but is the strongest region of excited-state absorption that is not partially canceled by the stimulated emission peaks (which are red-shifted compared to ^{F}**Ir**•**L**^{Me}). The excited-state lifetime as determined by decay of the TA signal in degassed CH_2Cl_2 matches the luminescence measurements under the same conditions, confirming that the excited-state absorption and the luminescence arise from the same ^{3}Ir excited state.

For the naphthyl-appended complexes ^{H}**Ir**•**L**^{14} and ^{H}**Ir**•**L**^{15} we find the same situation, that is, the excited-state lifetimes obtained from the TA spectra and from luminescence measurements under the same conditions are similar (Table 4, Figure 6a). The lengthening of these lifetimes to ∼10 μs

dx.doi.org/10.1021/ic401410g | *Inorg. Chem.* 2013, 52, 10500−10511

Table 4. Summary of Excited State Lifetimes from Luminescence and Transient Absorption Measurements[a]

	CH_2Cl_2/air-equilibrated	CH_2Cl_2/degassed	
	luminescence	luminescence[c]	transient absorption
^{H}Ir•L^{Me}	180 ns	1.1, 2.2 μs	1.5, 2.4 μs
^{H}Ir•L^{14}	670 ns	2, 11 μs	6.2, 15.9 μs
^{H}Ir•L^{15}	690 ns	3, 8 μs	5.4, 10.8 μs
^{H}Ir•L^{14}•Eu	160 ns, 70 ns[b]	0.7 μs	1.0, 5.7 μs
		5.9 μs	
		700 μs (Eu decay)	
^{H}Ir•L^{15}•Eu	170 ns, 60 ns[b]	0.1 μs	0.3 μs, 2.9 μs
		2 μs	
		700 μs (Eu decay)	
^{F}Ir•L^{Me}	600 ns	1.4, 2.4 μs	1.7, 2.6 μs
^{F}Ir•L^{14}	~500 ns[d]	1.4 μs	**1 μs (^{3}nap rise)**
			17 μs (^{3}nap decay)
			100 μs (^{3}nap decay)
^{F}Ir•L^{15}	~500 ns[d]	1.1 μs	**1.1 μs (^{3}nap rise)**
			18 μs (^{3}nap decay)
			62 μs (^{3}nap decay)
^{F}Ir•L^{14}•Eu	not measured	0.8 μs (^{3}Ir decay)	**1.3 μs (^{3}nap rise)**
		8.6 μs (Eu rise)	7.6 μs (^{3}nap decay)
		560 μs (Eu decay)	
^{F}Ir•L^{15}•Eu	not measured	1.1 μs (^{3}Ir decay)	**1.5 μs (^{3}nap rise)**
		15 μs (Eu rise)	15 μs (^{3}nap decay)
		460 μs (Eu decay)	

[a]Decays are in normal type; rise times are in bold type. [b]Also present was a small ≈700 ns component (<10% of total emission intensity) ascribable to traces of the free Ir complex as part of the equilibrium in Scheme 1. [c]Ir-based decay measured at around 500 nm (or as mentioned in the figures); Eu-based decay measured at 615 nm. [d]Very weak Ir-based emission arising from a minor conformer in which the Ir-based emission is not quenched by the naphthyl group; the majority of the Ir-based emission is assumed to be completely quenched (see main text).

compared to ^{H}Ir•L^{Me} ($\tau \sim 2$ μs) may be ascribed again to the reservoir effect as discussed earlier:[9] that is, the excited state lifetime of the ^{3}Ir unit is lengthened by close interaction with the naphthyl unit which has a similar excited state energy. The appearance of the emission spectra of ^{H}Ir•L^{14} and ^{H}Ir•L^{15} confirm that the emissive excited state is still ^{3}Ir in character.

The fluorinated complexes ^{F}Ir•L^{14} and ^{F}Ir•L^{15} bearing the napthyl group however show significantly different behavior from that of their nonfluorinated analogues discussed above. As described earlier, the ^{3}Ir luminescence intensity is largely (>90%) quenched by the presence of the naphthyl group. Emission lifetimes in degassed CH_2Cl_2 (~1 μs in each case) correspond with the very weak decay components of ≈500 ns obtained in air-equilibrated CH_2Cl_2 arising from small amounts of unquenched "open" conformers, see above. We expect there also to be a dominant folded conformer in which ^{3}Ir-based emission is completely quenched. In agreement with this, the TA spectra in each case show the presence of a much longer-lived excited state whose lifetime does not correspond to the weak ^{3}Ir-based luminescence (Figure 6b).

For ^{F}Ir•L^{14} the decay of the excited state absorption at 420 nm now shows three components with lifetimes spanning 2 orders of magnitude. The first is a *grow-in* of 1 μs which can be ascribed to population of the ^{3}nap state by ^{3}Ir→nap energy-transfer which is now possible because of the higher excited state energy of the ^{3}Ir state arising from the fluorination of the ligands. As required, the lifetime of the grow-in matches the luminescence decay component observed for ^{F}Ir•L^{14} under the same conditions. Once formed, decay of the ^{3}nap state is bi-exponential with lifetime values of τ = 17 and 100 μs, consistent with the existence of two major conformers. These long excited state lifetimes, especially the dominant 100 μs component, are entirely consistent with the values expected for triplet states of organic aromatic groups. The fact that these lifetimes are associated with a triplet excited state is confirmed by the fact that they are sensitive to the presence of O_2 (in air-equilibrated solution these lifetimes are reduced to 0.5 and 1.5 μs); in addition, this triplet state cannot be ^{3}Ir as clearly shown by the luminescence behavior. Thus we are seeing ≈1 μs growth and slow (17 and 100 μs) decay of the ^{3}nap state following ^{3}Ir→nap energy-transfer. ^{F}Ir•L^{15} shows exactly similar behavior with the excited-state absorption at 420 nm having a grow-in of 1.1 μs, and two slower decay components of τ = 18 and 62 μs consistent with deactivation of the ^{3}nap state (Figure 6b). The conclusion again is that the TA signal corresponds to formation and then slow decay of a ^{3}nap excited state following ^{3}Ir→nap energy-transfer.

To conclude this section, it is clear that ^{H}Ir•L^{n} and ^{F}Ir•L^{n} (n = 14, 15) behave differently from one another. In the former pair of complexes the excited state observed in the TA spectra is the same as the luminescent excited state and is the expected ^{3}Ir state with a modest increase in luminescence lifetime arising from the reservoir effect. In the latter pair, there is a long-lived nonemissive triplet excited state which is clearly not the luminescent ^{3}Ir state; it grows in (≈1 μs) and then decays slowly with lifetimes of up to 100 μs. This must be the ^{3}nap state, generated by ^{3}Ir→nap energy-transfer, which has become possible because of the high energy of the ^{3}Ir state when the phenylpyridine ligands are fluorinated. Note that the excitation (at 355 nm) is in a region where naphthalene does not absorb directly, so the ^{3}nap state can *only* be populated by energy-transfer from the initially generated ^{3}Ir-based excited state of ^{F}Ir•L^{14} and ^{F}Ir•L^{15}.

dx.doi.org/10.1021/ic401410g | Inorg. Chem. 2013, 52, 10500−10511

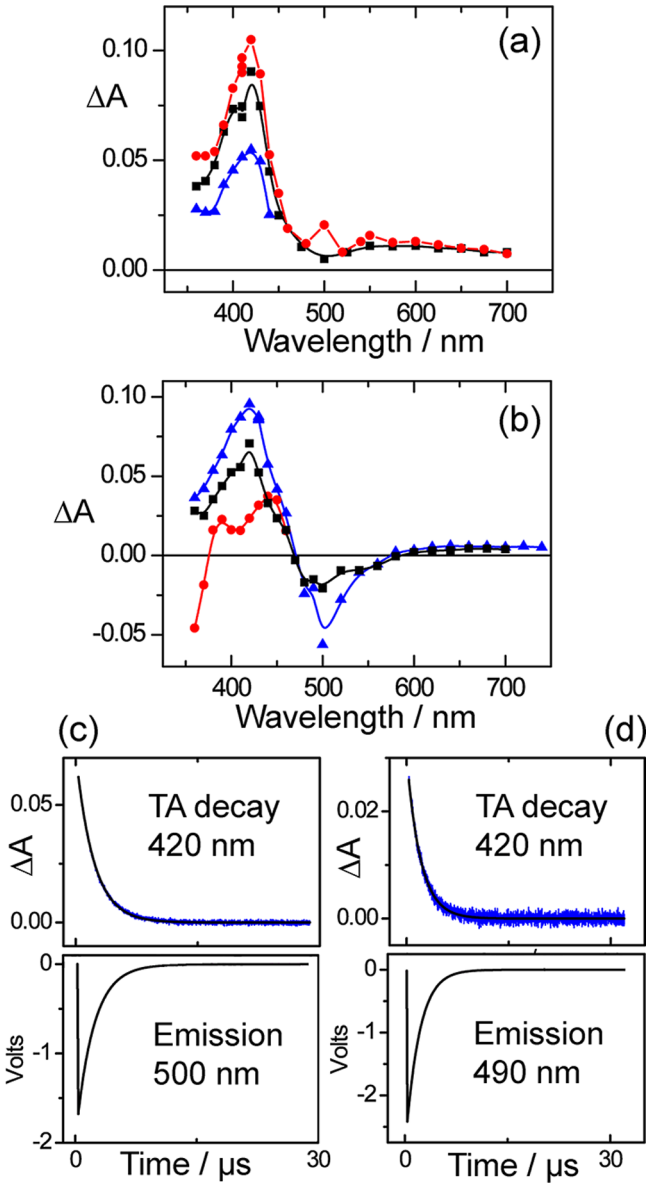

Figure 5. Transient absorption spectra of fluorinated (a) and nonfluorinated (b) compounds recorded in CH_2Cl_2 at RT, following excitation with a 355 nm, ~7 ns laser pulse, recorded immediately after excitation. (a) Black squares, ^{F}**Ir•L**^{14}; blue triangles, ^{F}**Ir•L**^{Me}; red circles, ^{F}**Ir•L**^{15}. (b) Black squares, ^{H}**Ir•L**^{14}; red circles, ^{H}**Ir•L**^{Me}; blue triangles, ^{H}**Ir•L**^{15}. Kinetic decays for transient absorption and emission signals, as indicated, for (c) ^{F}**Ir•L**^{Me} and (d) ^{H}**Ir•L**^{Me}; solid black lines represents the fit to the data with the parameters listed in Table 4.

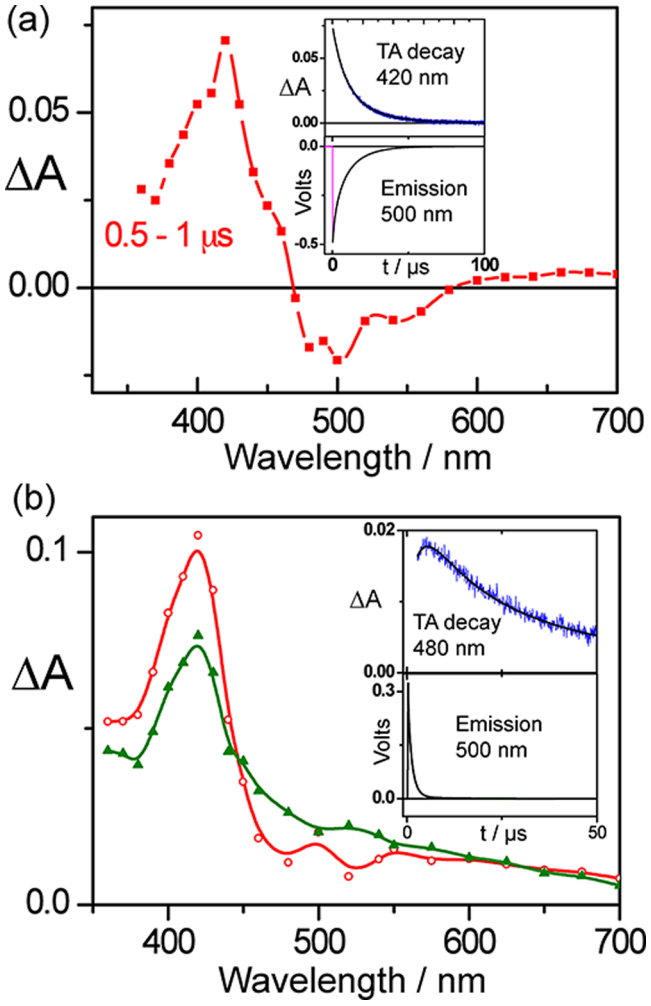

Figure 6. Transient absorption spectra and associated transient absorption and emission kinetics for (a) ^{H}**Ir•L**^{14} (averaged between 500 and 1000 ns after excitation), and (b) ^{F}**Ir•L**^{15} (reconstructed excited state spectra obtained by a global fit), both in deaerated CH_2Cl_2 at RT, following a 355 nm, ~7 ns laser pulse. The solid black line represents the fit to the data with the parameters listed in Table 4. On panel (b), the two spectra shown correspond to the early time ^{3}Ir-based excited state (open circles, red) and to the subsequently formed ^{3}nap state (triangles, green). In (a) the correspondence between the relatively long luminescence and TA decay lifetimes is clear; in (b) the much shorter luminescence decay correlates with the *rise time* of the TA spectrum, and the slow TA decay does not have a matching luminescence component; see main text.

2.3. Luminescence Properties of Ir/Naphthyl/Eu Three-Component Complexes. As described in the introduction our motivation here was to see if the spatial and energetic intermediacy of a ^{3}nap state between ^{3}Ir (energy-donor) and Eu (energy-acceptor) components facilitated the d→f energy-transfer process. We investigated this in two ways. First we performed luminescence titrations in air-equilibrated CH_2Cl_2 in which small portions of $[Eu(hfac)_3(H_2O)_2]$ were added to the samples of ^{F}**Ir•L**^{1n} and ^{H}**Ir•L**^{1n} to form ^{F}**Ir•L**^{n}**•Eu** and ^{H}**Ir•L**^{n}**•Eu** respectively (n = 14, 15 in both cases). During these titrations we monitored the degree of quenching by the $\{Eu(hfac)_3\}$ unit of the Ir-based luminescence, and also the appearance of sensitized Eu-centered emission. Plots of Ir-based emission intensity vs concentration of added $[Eu(hfac)_3(H_2O)_2]$ (showing the steady quenching during the titration), and of Eu-based emission intensity vs concentration of added $[Eu(hfac)_3(H_2O)_2]$ (showing the steady grow-in during the titration), fit to 1:1 binding isotherms and give binding constants for the equilibrium in Scheme 1 of about 2×10^4 M^{-1} in agreement with previous work.[2e] Second, we performed TA measurements in deaerated CH_2Cl_2 on samples of ^{F}**Ir•L**^{n} and ^{H}**Ir•L**^{n} (n = 14, 15) to which an excess of $[Eu(hfac)_3(H_2O)_2]$ was added, to form the adducts ^{F}**Ir•L**^{n}**•Eu** and ^{H}**Ir•L**^{n}**•Eu** respectively via the equilibrium in Scheme 1.

(i). ^{H}***Ir•L***^{14}***•Eu and*** ^{H}***Ir•L***^{15}***•Eu.*** Addition of small portions of $[Eu(hfac)_3(H_2O)_2]$ to a solution of ^{H}**Ir•L**^{14} (6.4×10^{-5} M in CH_2Cl_2) resulted in evolution of the steady-state

dx.doi.org/10.1021/ic401410g | *Inorg. Chem.* 2013, 52, 10500−10511

luminescence spectra as shown in Figure 7. Excitation was into the low-energy tail of the MLCT absorption of the Ir unit at

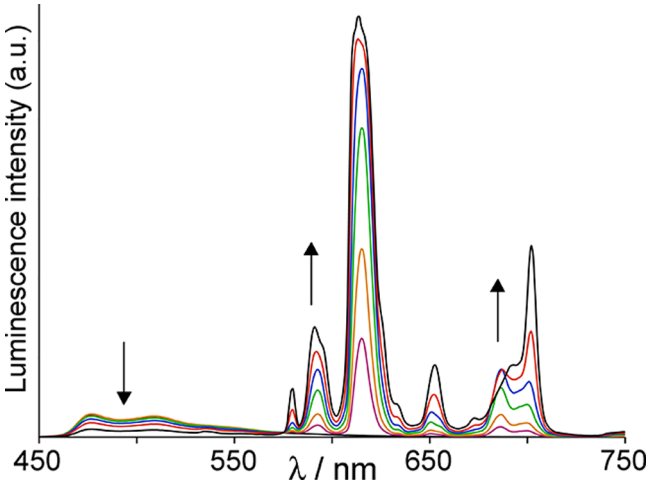

Figure 7. Changes in luminescence spectra (λ_{exc} 380 nm) recorded during titration of ^{H}**Ir•L**^{14} (6.4×10^{-5} M) with $[Eu(hfac)_3(H_2O)_2]$ (1.4 mM; up to 3 equiv compared to ^{H}**Ir•L**^{14}) in CH_2Cl_2 to form the ^{H}**Ir•L**^{14}**•Eu** dyad, showing the decay of Ir-based emission (450−600 nm) and the rise of sensitized Eu-based emission (570−720 nm) as ^{H}**Ir•L**^{14}**•Eu** forms according to Scheme 1.

380 nm. The $\{Eu(hfac)_3\}$ unit does not absorb in this region, which has two important consequences. First it means that the absorbance at the excitation wavelength is purely into the Ir chromophore and remains constant during the titration, such that changes in luminescence intensity reflect real changes in emission quantum yields. It also means that any emission seen from the $\{Eu(hfac)_3\}$ unit can only arise from d→f energy-transfer in the intact complex ^{H}**Ir•L**^{14}**•Eu**: any free $[Eu(hfac)_3(H_2O)_2]$ (cf. the equilibrium in Scheme 1) will not absorb light and therefore will not interfere with the emission spectra.

As ^{H}**Ir•L**^{14}**•Eu** formed during the titration, according to Scheme 1, the Ir-based emission in the 450−600 nm region steadily decreased, and this quenching was accompanied by appearance of intense Eu-based emission displaying the usual sequence of $^5D_0 \rightarrow {}^7F_n$ components between 570 and 720 nm. No significant changes were observed after addition of about 3 equiv of $[Eu(hfac)_3(H_2O)_2]$. At this end-point the Ir-based emission was reduced in intensity by 65% because of Ir→Eu energy-transfer in the dyad.

Time-resolved measurements on the residual Ir-based luminescence, using a 475−525 nm bandpass filter to reject the intense Eu-based sensitized emission which would otherwise interfere, showed that it comprised at least three exponential components. A weak component with $\tau \approx 0.7$ μs can be ascribed to traces of residual ^{H}**Ir•L**^{14} (cf. Scheme 1). Two additional shorter components with $\tau \approx 160$ and 70 ns were needed to give a satisfactory fit to the luminescence decay curve. These may be ascribed to partial quenching of the ^{3}Ir emission by Ir→Eu energy-transfer in two (at least) different conformers of ^{H}**Ir•L**^{14}**•Eu**, with energy-transfer rate constants of the order of 10^7 s^{-1}. In contrast use of (nonquenching) $[Gd(hfac)_3(H_2O)_2]$ in place of $[Eu(hfac)_3(H_2O)_2]$ as a control, because Gd(III) does not have any low-lying excited states that can act as energy-acceptors from either the ^{3}Ir or ^{3}nap states, resulted in a slight *increase* of about 20% in the Ir-based emission intensity by the end of the titration; this was accompanied by a marginal increase in the ^{3}Ir emission lifetime from 670 to 700 ns. This presumably occurs because addition of the $\{Gd(hfac)_3\}$ unit to the pendant pyrazolyl-pyridine site of ^{H}**Ir•L**^{14} to give ^{H}**Ir•L**^{14}**•Gd** results in rigidification of the complex and the consequent loss of some nonradiative deactivation pathways that were associated with molecular vibrations.

Titration of ^{H}**Ir•L**^{15} with $[Eu(hfac)_3(H_2O)_2]$ and $[Gd(hfac)_3(H_2O)_2]$ under the same conditions (6.4×10^{-5} M in air-equilibrated CH_2Cl_2) showed exactly similar behavior. Formation of ^{H}**Ir•L**^{15}**•Eu** was accompanied by 65% quenching of the ^{3}Ir emission intensity of ^{H}**Ir•L**^{15} following incomplete Ir→Eu energy-transfer. Strong sensitized Eu-based emission grew in during the titration as ^{H}**Ir•L**^{15}**•Eu** formed. The residual ^{3}Ir-based emission had lifetime components of about 170 and 60 ns arising from Ir→Eu energy-transfer in different conformers of ^{H}**Ir•L**^{15}**•Eu**. Formation of ^{H}**Ir•L**^{15}**•Gd** as a control experiment was accompanied by a slight increase (≈10%) of Ir-based emission intensity compared to free ^{H}**Ir•L**^{15}, with a change in lifetime from 690 to 740 ns, presumably because of rigidification of the complex when $\{Gd(hfac)_3\}$ binds, as described above.

For both ^{H}**Ir•L**^{14}**•Eu** and ^{H}**Ir•L**^{15}**•Eu**, therefore, the behavior is similar to what we have observed with related Ir/Eu dyads but using simple phenyl spacers in place of naphthyl in the bridging ligand.[2e] Ir→Eu energy-transfer occurs with some quenching of the Ir-based emission, to an extent which will depend on the separation between the metal ions in the ensemble of conformers of these flexible complexes. From the residual ^{3}Ir emission components in the Ir/Eu dyads (∼ 100 ns) we can estimate Ir→Eu energy-transfer rates of the order of 10^7 s^{-1} (the obvious difficulties in fitting multiexponential decays mean that one should not be too precise about these values). We showed earlier that Förster energy-transfer between these chromophores could only be significant over a distance of <3 Å given the very small donor/acceptor Förster spectroscopic overlap.[2e] In contrast Dexter-type energy-transfer is possible over the distances required in ^{H}**Ir•L**^{14}**•Eu** and ^{H}**Ir•L**^{15}**•Eu** by means of a weak electronic coupling that is facilitated by π-stacking of the type that we observed in the crystal structures described earlier,[2e] even though here is no evidence for a separate ^{3}nap excited state being involved as an intermediate.

Given that Eu-based emission occurs only as a consequence of Ir→Eu energy-transfer under these conditions, we might expect to see a grow-in for the Eu-based emission in both ^{H}**Ir•L**^{14}**•Eu** and ^{H}**Ir•L**^{15}**•Eu**. However any grow-in of Eu-based emission at 615 nm will be masked by the decay in the tail of the residual Ir-based emission intensity at the same wavelength which must be synchronous. Accordingly time-resolved measurements at 615 nm did not reveal a grow-in associated with sensitization of Eu-based emission but this is to be expected.

(ii). ^{F}***Ir•L***^{14}***•Eu*** *and* ^{F}***Ir•L***^{15}***•Eu.*** Luminescence titrations using the fluorinated complexes ^{F}**Ir•L**^{n} (n = 14, 15), having a higher-energy ^{3}Ir state, were performed in air-equilibrated CH_2Cl_2 by addition of small portions of $[Eu(hfac)_3(H_2O)_2]$ in the same way as described above, until no further significant changes were observed (after addition of about 4 equiv of $[Eu(hfac)_3(H_2O)_2]$). The results using ^{F}**Ir•L**^{14} are shown in Figure 8. Compared to the nonfluorinated ^{H}**Ir•L**^{14} system the weakness of the initial Ir-based luminescence is obvious, and this is quenched further (about 30% additional reduction in intensity) as ^{F}**Ir•L**^{14}**•Eu** forms. Time-resolved analysis of this residual Ir-based emission did not yield useful results, which

dx.doi.org/10.1021/ic401410g | *Inorg. Chem.* 2013, 52, 10500−10511

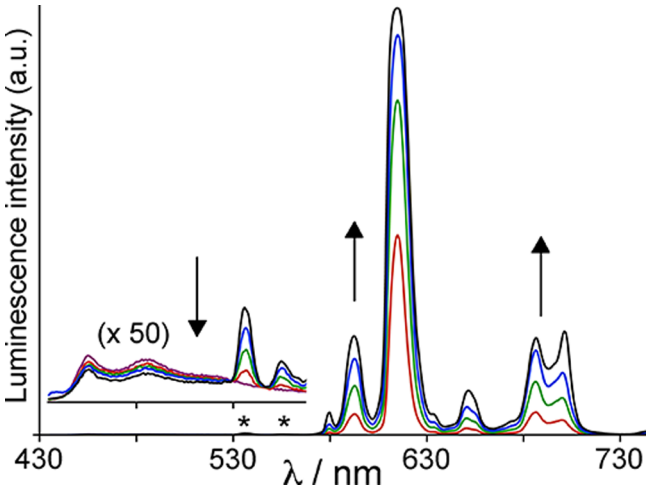

Figure 8. Changes in luminescence spectra (λ_{exc} 380 nm) recorded during titration of ^{F}**Ir•L**^{14} (6.5×10^{-5} M) with $[Eu(hfac)_3(H_2O)_2]$ (0.82 mM; up to 3 equiv compared to ^{F}**Ir•L**^{14}) in CH_2Cl_2 to form the ^{F}**Ir•L**^{14}**•Eu** dyad, showing the decay of the very weak Ir-based emission (450−600 nm) and the rise of sensitized Eu-based emission (570−720 nm) as ^{H}**Ir•L**^{14}**•Eu** forms according to Scheme 1. The two very weak, sharp emission peaks at 535 and 664 nm (labeled *) are traces of Eu-based emission originating from the $^5D_1$ state rather than $^5D_0$.

is unsurprising given both its weakness and likely multiexponential behavior arising from different conformers. However from the intensity changes we can say that some additional Ir→Eu energy-transfer is occurring, in addition to the predominant ^{3}Ir→nap energy-transfer which results in such weak Ir-based emission in the first place.

Despite the weakness of emission from ^{F}**Ir•L**^{14} and ^{F}**Ir•L**^{15} because of ^{3}Ir→nap energy-transfer, strong sensitized Eu-based emission still occurs in ^{F}**Ir•L**^{14}**•Eu** and ^{F}**Ir•L**^{15}**•Eu**. This implies that in both cases the intermediate ^{3}nap state, with its long excited-state lifetime, is acting as the energy-donor to Eu(III) in a *two-step* ^{3}Ir→^{3}nap→Eu energy-transfer sequence. Time-resolved luminescence measurements (degassed CH_2Cl_2) on ^{F}**Ir•L**^{14}**•Eu** at 615 nm revealed a clear rise-time of 8.6 μs for the sensitized Eu-based emission, which is not obscured by synchronous decay of Ir-based emission as was the case with ^{H}**Ir•L**^{14}**•Eu**, because the Ir-based emission of ^{F}**Ir•L**^{14}**•Eu** decays on a faster time scale and is so much weaker. This rise-time of the Eu-based emission correlates well with the 7.6 μs decay of the ^{3}nap state according to the TA spectra (see next section) and is therefore completely consistent with sensitization via ^{3}nap→Eu energy-transfer. The lifetime of the Eu-based emission is characteristically very long (560 μs).

Similar behavior is shown on formation of ^{F}**Ir•L**^{15}**•Eu**, with about a 30% reduction in the intensity of the very weak emission of ^{F}**Ir•L**^{15} when the $\{Eu(hfac)_3\}$ unit bonds at the secondary pyrazolyl-pyridine site, and the appearance of sensitized Eu-based emission of comparable intensity. Again the rise-time observed for sensitized Eu-based emission (15 μs) matches well the decay of the ^{3}nap state that is observed in the TA spectrum under the same conditions (see next section), signaling a ^{3}nap→Eu energy-transfer process following selective excitation of the Ir-based component. Thus a two-step ^{3}Ir→^{3}nap→Eu energy-transfer sequence is again operative.

2.4. Transient Absorption Measurements on Ir/Naphthyl/Eu Three-Component Complexes. TA measurements were particularly useful at clarifying the sequential nature of the energy-transfer processes and were performed in degassed CH_2Cl_2. As mentioned earlier the excited-state absorption of ^{H}**Ir•L**^{14} (arising from the ^{3}Ir excited state) shows complex decay kinetics which can be approximated with two components having $\tau \approx 6$ and 16 μs under these conditions. In the presence of 5 equiv of $[Eu(hfac)_3(H_2O)_2]$, to convert ^{H}**Ir•L**^{14} to ^{H}**Ir•L**^{14}**•Eu**, the TA spectrum retains a similar appearance, but the excited state absorption at 420 nm decays more quickly with τ = 1.0 and 5.7 μs, in good agreement with luminescence lifetimes measured on the same sample under the same conditions (Table 4). This is consistent with the partial quenching of the ^{3}Ir-based emission intensity that we observed in the luminescence titration experiment. The correspondence of the excited-state lifetimes from the TA spectrum and the ^{3}Ir-based luminescence lifetimes again implies a simple ^{3}Ir→Eu energy-transfer process as we saw for related Ir/Eu dyads, without the intermediacy of a nonemissive ^{3}nap state that is too high in energy to participate. From these lifetime values we can estimate ^{3}Ir→Eu energy-transfer rates in the range 10^5−10^6 s^{-1} for those conformers whose excited-state decay is clearly visible by the TA method.

We can therefore detect from the TA decay kinetics for ^{H}**Ir•L**^{14}**•Eu** energy-transfer processes that are considerably slower than the values of about 10^7 s^{-1} that were estimated from luminescence measurements performed during the titrations. We emphasize however that each technique may reveal different processes. Fast ^{3}Ir→Eu energy-transfer processes based on more compact conformations of the complexes may be difficult to detect by TA measurements if these are present in only small amounts, because in this case the TA signal will be dominated by the more abundant longer-lived ^{3}Ir component from slow energy-transfer. Conversely a slow energy-transfer process, even if it is the dominant pathway, could easily be undetectable by luminescence measurements: energy-transfer with a rate constant of 10^5 s^{-1} would only reduce the ^{3}Ir-based emission lifetime from (say) 700 ns for a free Ir complex in air-equilibrated solvent to about 680 ns in a Ir/Eu dyad, a difference which is much less than the experimental uncertainty. We conclude that the combination of TA and luminescence measurements on ^{H}**Ir•L**^{14}**•Eu** reveal a range of ^{3}Ir→Eu energy-transfer processes with time scales spanning the range 10^5−10^7 s^{-1} in different conformers.

^{H}**Ir•L**^{15}**•Eu** shows similar behavior: on conversion of ^{H}**Ir•L**^{15} to ^{H}**Ir•L**^{15}**•Eu**, the excited-state absorption at 420 nm which signals formation of the ^{3}Ir state decays more quickly with the longest component being reduced from 11 to 3 μs in degassed CH_2Cl_2, and a similar conclusion of direct ^{3}Ir→Eu energy-transfer applies.

The kinetics of the TA spectrum of ^{F}**Ir•L**^{14} in degassed CH_2Cl_2 showed a rise-time of 1 μs for sensitization of the ^{3}nap state, followed by slow ($\tau \approx 17$ and 100 μs) decays whose lifetimes had no counterpart in the weak ^{3}Ir luminescence, consistent with formation of a nonemissive ^{3}nap state (cf. the similar behavior of ^{F}**Ir•L**^{15} illustrated in Figure 6b). In the presence of 5 equiv of $[Eu(hfac)_3(H_2O)_2]$ to generate ^{F}**Ir•L**^{14}**•Eu** in situ according to Scheme 1, the ^{3}nap lifetime is reduced to 7.6 μs by ^{3}nap→Eu energy-transfer, as manifested by transient absorption studies (Figure 9). Importantly, this 7.6 μs decay component for the ^{3}nap state matches very well the 8.6 μs rise-time observed for the sensitized Eu-based emission at 615 nm, confirming the occurrence of a ^{3}nap→Eu

dx.doi.org/10.1021/ic401410g | Inorg. Chem. 2013, 52, 10500−10511

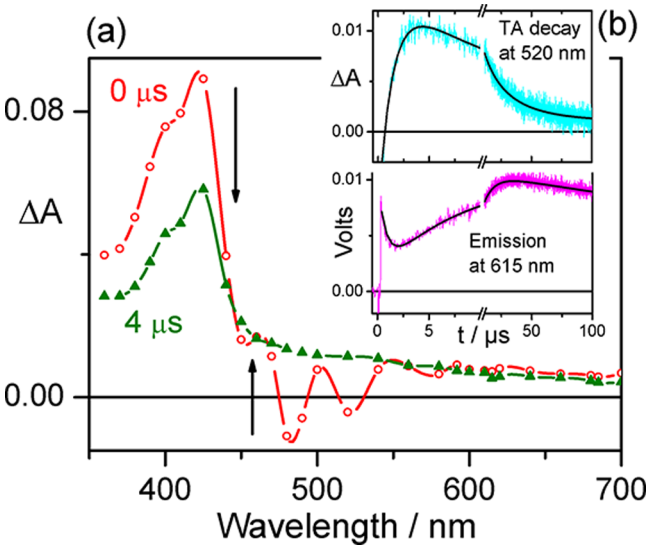

Figure 9. Transient absorption spectra of ^{F}**Ir•L^{14}•Eu** in CH_2Cl_2 at RT. (a) Transient absorption spectra at 0 and 4 μs after 355 nm excitation, reconstructed using global fit analysis. (b) Kinetic traces for transient absorption decay (top) and emission (bottom) at the wavelengths specified. The solid black line represents the two-exponential (TA) and the three-exponential (emission) fit to the data with the parameters listed in Table 4.

energy-transfer process and the intermediacy of the ^{3}nap state in the two-step ^{3}Ir→^{3}nap→Eu energy-transfer sequence (Figure 9, 10). Further proof was obtained by repeating the

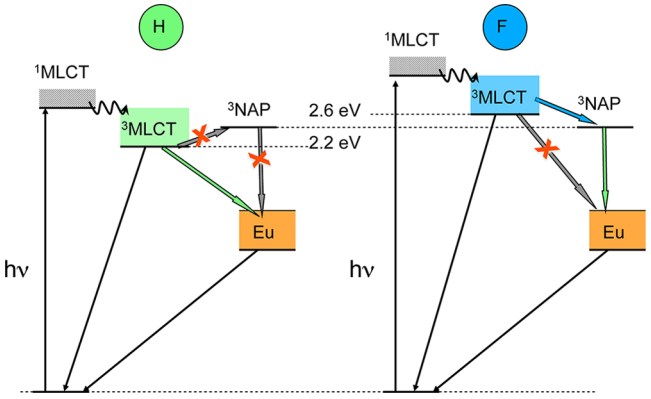

Figure 10. Outline photophysical scheme summarizing how the differing energy of the ^{3}Ir states between the ^{H}**Ir** and ^{F}**Ir** complexes results in different energy-transfer pathways to the Eu(III) center.

above measurements after admitting air to the CH_2Cl_2 sample solution. This resulted in the ^{3}nap lifetimes obtained from the TA spectrum being reduced to ≈0.2 and 1.2 μs because of $^3O_2$ quenching, and also resulted in the grow-in of Eu-based emission at 615 nm being reduced to 1.5 μs in the time-resolved luminescence measurements. Again we have a good correspondence between the main ^{3}nap decay component (1.2 μs) and the rise-time of sensitized Eu-based emission (1.5 μs). For ^{F}**Ir•L^{15}•Eu** the sensitization of Eu emission by the ^{3}nap state is equally clear. The long-lived ^{3}nap state of ^{F}**Ir•L^{15}** ($\tau \approx 18, 62$ μs) is shortened to 15 μs when ^{F}**Ir•L^{15}•Eu** forms, and again the key point is that this decay of the ^{3}nap state perfectly matches the 15 μs rise-time of the sensitized Eu emission.

For both ^{F}**Ir•L^{14}•Eu** and ^{F}**Ir•L^{15}•Eu**, therefore, we can directly observe both steps of the ^{3}Ir→^{3}nap→Eu energy-transfer sequence from the rise and decay of the intermediate ^{3}nap state in the TA spectrum (Figure 9). The first (^{3}Ir→nap) energy-transfer step is shown by quenching of ^{3}Ir luminescence, and the *ca.* 1 μs grow-in of the ^{3}nap state matches the residual ^{3}Ir decay component. The second (^{3}nap→Eu) energy-transfer step is again clearly shown by the grow-in of sensitized Eu-based emission which closely matches the ^{3}nap decay rate. The schematic photophysical diagram summarizing two different mechanisms of energy transfer in shown in Figure 10. Remarkably, fluorination of the ancillary ligand, which only affects the energy of the energy donating antenna state by <0.4 eV, induces a complete switch between the two mechanisms of d-f energy transfer: the one step ^{3}Ir→Ln energy transfer in the nonfluorinated complexes, and the two-step ^{3}Ir→^{3}nap→Eu process, mediated by the naphthalene spacer, in the fluorinated complexes.

CONCLUSIONS

We have prepared two sets of complexes containing an Ir(phenylpyridine)/naphthyl/Eu(hfac)$_3$ sequence of photoactive units. The energies of the ^{3}naphthyl and Eu-based excited states do not change significantly between members of the series, but the ^{3}Ir-based excited state may lie at 22,200 cm^{-1} or 21,400 cm^{-1} according to whether the phenylpyridine ligands are fluorinated or not. In the nonfluorinated complexes ^{H}**Ir•L^{n}** (n = 14, 15) the ^{3}Ir state is too low in energy to be quenched by the ^{3}nap state, with the result that these complexes show typical ^{3}Ir-based luminescence and their Eu(hfac)$_3$ adducts ^{H}**Ir•L^{n}•Eu** show normal ^{3}Ir→Eu energy-transfer in which the ^{3}Ir-based emission is substantially quenched. The Dexter-type energy-transfer process is facilitated by aromatic stacking between the components in which the naphthyl group is involved, but there is no ^{3}nap intermediate state. A range of energy-transfer rate constants (≈ 10^5–10^7 s^{-1}) detected by a combination of time-resolved luminescence and TA spectroscopic methods is consistent with a range of conformers with different Ir···Eu separations and energy-transfer pathways.

In contrast, in the fluorinated complexes ^{F}**Ir•L^{14}** and ^{F}**Ir•L^{15}** the ^{3}Ir state is now high enough in energy to be quenched by ^{3}Ir→nap energy-transfer generating a long-lived ^{3}nap state. This means that in the Eu(hfac)$_3$ adducts ^{F}**Ir•L^{14}•Eu** and ^{F}**Ir•L^{15}•Eu** there is now a two-step ^{3}Ir→^{3}nap→Eu energy-transfer sequence, with the intermediate ^{3}nap state being sensitized by the ^{3}Ir donor and passing its energy on to the Eu(hfac)$_3$ unit, with the rise-time of sensitized Eu(III) luminescence matching the decay time of the ^{3}nap state in each case. Thus, slightly increasing the ^{3}Ir energy by fluorination of the phenylpyridine ligands results in a fundamentally different energy-transfer pathway leading to sensitized Eu(III)-based emission. This finding demonstrates the first example of such a switch in d/f systems, and illustrates further how fine-tuning of electronic structure can manipulate energy transfer processes.

EXPERIMENTAL DETAILS

General Details. The following compounds were prepared according to published methods: the ligands L^{Me},[12] L^{14},[8a] and L^{15};[8b] the dimers [Ir(phpy)$_2$(μ–Cl)]$_2$ based on unsubstituted 2-phenylpyridine and the fluorinated analogue 2-(2,4-difluorophenyl)-pyridine;[13] and Eu(hfac)$_3$(H$_2$O)$_2$.[14] Electrospray mass spectra were recorded using a Micromass LCT instrument; ^{1}H NMR spectra were recorded on a Bruker Avance-2 400 MHz instrument. UV/vis

dx.doi.org/10.1021/ic401410g | Inorg. Chem. 2013, 52, 10500–10511

absorption spectra were measured on a Cary 50 spectrophotometer, and steady-state luminescence spectra on a Jobin-Yvon Fluoromax 4 fluorimeter using air-equilibrated CH_2Cl_2 solutions at room temperature. Ir-based emission lifetimes measured during the titrations with $Eu(hfac)_3(H_2O)_2$ were measured using the time-correlated single photon counting technique with an Edinburgh Instruments "Mini-τ" luminescence lifetime spectrometer, equipped with a 405 nm pulsed diode laser as excitation source and a Hamamatsu-H5773−03 PMT detector; the lifetimes were calculated from the measured data using the supplied software. Luminescence quantum yields were calculated by comparing areas of corrected luminescence spectra, from isoabsorbing solutions, following the method described by Demas and Crosby[15] and using *fac*-[Ir(ppy)$_3$] (ppy = anion of 2-phenylpyridine) as a standard.[16]

Synthesis of the Complexes. The complexes (see Chart 1) were prepared using the same method; the synthesis of ^{F}**Ir•L**^{14} given here is typical. A solution of the ligand L[14] (0.038 g, 85 μmol, 1.3 equiv with respect to Ir) was dissolved in CH_2Cl_2/MeOH (3:1, v/v) under N_2. To this was added a solution of the dimer $[Ir(F_2phpy)_2(\mu\text{-}Cl)]_2$ (0.040 g, 33 μmol) in CH_2Cl_2. The mixture was heated to 50 °C overnight under N_2 and in the dark. The mixture was cooled to room temperature and the solvent removed. Water and saturated KPF_6 solution (20 cm^3) was added, and the resulting two-phase mixture was separated; the aqueous residue was further extracted with several portions of CH_2Cl_2 (3 × 30 cm^3). The combined organic fractions were dried using Na_2SO_4 and the solvent removed. The yellow powder was purified by column chromatography on silica gel using MeCN and 1% aqueous KNO_3; complex ^{F}**Ir•L**^{14} was the second yellow band to elute from the column. Fractions containing the pure product were combined and reduced in volume; excess KNO_3 was precipitated by addition of CH_2Cl_2 and filtered off. Evaporation of the resultant solution to dryness afforded pure ^{F}**Ir•L**^{14} as its nitrate salt.

Characterization Data for ^{F}***Ir•L*^{14}. ^{1}H NMR (400 MHz, $CDCl_3$): δ 8.72 (1H, d), 8.49 (1H, d), 8.25 (1H, d), 8.13−7.99 (5H, m), 7.85 (2H, t), 7.66 (1H, t), 7.64−7.53 (3H, m), 7.48−7.37 (4H, m), 7.33−7.29 (4H, m), 7.04 (1H, s), 6.87 (1H, t), 6.50 (1H, t), 6.22 (1H, d), 5.99 (1H, d), 5.86−5.56 (5H, m), 5.33−5.28 (2H, m). ESMS: m/z 1015 $(M - NO_3)^+$. Anal. Calc. for $C_{50}H_{34}N_8F_4IrNO_3\cdot0.5CH_2Cl_2$: C 54.2, H 3.2, N 11.3%. Found: C 53.8, H 3.1, N 11.3%.

Characterization Data for ^{F}***Ir•L*^{15}. ^{1}H NMR (400 MHz, $CDCl_3$): δ 8.69 (1H, d), 8.54 (1H, d), 8.24 (1H, d), 8.14−8.09 (2H, m), 8.0 (1H, d), 7.88−7.77 (4H, m), 7.68 (1H, d), 7.65 (1H, d), 7.51 (1H, d), 7.42−7.25 (7H, m), 7.20 (1H, d), 7.13 (1H, d), 6.94−6.90 (2H, d), 6.61 (1H, t), 6.50 (1H, t), 5.95−5.74 (4H, m), 5.64−5.59 (2H, m), 5.37−5.30 (2H, m). ESMS: m/z 1015 $(M - NO_3)^+$. Anal. Calc. for $C_{50}H_{34}N_8F_4IrNO_3\cdot0.5CH_2Cl_2$: C 54.2, H 3.2, N 11.3%. Found: C 53.7, H 3.2, N 11.1%.

Characterization Data for ^{H}***Ir•L*^{14}. ^{1}H NMR (400 MHz, $CDCl_3$): δ 8.69 (1H, d), 8.41 (1H, d), 8.07−8.00 (3H, m), 7.95−7.92 (2H, m), 7.85 (1H, d), 7.78 (2H, m), 7.70 (1H, d), 7.59−7.48 (5H, m), 7.42 (1H, d), 7.32 (2H, t), 7.24 (2H, q), 7.14 (1H, d), 7.03 (1H, d), 6.98−6.94 (2H, m), 6.84 (1H, t), 6.79 (1H, t), 6.59 (1H, t), 6.45 (1H, d), 6.38 (1H, d), 6.26−6.21 (2H, m), 5.98 (1H,d), 5.89 (1H, d), 5.80 (1H, d), 5.71 (1H, d), 5.60 (1H, d), 5.51 (1H, d). ESMS: m/z 943 $(M - NO_3)^+$. Anal. Calc. for $C_{50}H_{38}N_8IrNO_3\cdot0.7CH_2Cl_2$: C 57.2, H 3.7, N 11.8%. Found: C 57.1, H 3.7, N 11.6%.

Characterization Data for ^{H}***Ir•L*^{15}. ^{1}H NMR (400 MHz, $CDCl_3$): δ 8.69 (1H, d), 8.46 (1H, d), 8.09−8.02 (2H, m), 7.97 (1H, d), 7.89−7.74 (5H, m), 7.69 (1H, d), 7.58−7.55 (2H, m), 7.47−7.43 (3H, m), 7.32−7.20 (5H, m), 7.06 (1H, d), 6.99−6.82 (3H, m), 6.81−6.60 (4H, m), 6.32−6.25 (2H, m), 6.22 (1H, d), 5.99 (1H, d), 5.91 (1H, d), 5.78 (1H, d), 5.70 (1H, d), 5.66−5.50 (2H, m). ESMS: m/z 943 $(M - NO_3)^+$. Anal. Calc. for $C_{50}H_{38}N_8IrNO_3\cdot0.7CH_2Cl_2$: C 57.2, H 3.7, N 11.8%. Found: C 57.2, H 4.0, N 12.0%.

Characterization Data for ^{F}***Ir•L*^{Me}. ^{1}H NMR (400 MHz, $CDCl_3$): δ 8.42 (1H, d), 8.38 (1H, d), 8.31 (1H, d), 8.11 (1H, t), 8.04 (1H, d), 7.88 (2H, m), 7.75 (2H, d), 7.50 (1H, d), 7.38 (1H, d), 7.34 (1H, t), 7.26 (1H, t), 7.11 (1H, t), 6.55 (2H, m), 5.70 (1H, d), 5.60 (1H, d), 3.45 (3H, s). ESMS: m/z 733 $(M - NO_3)^+$. Anal. Calc. for $C_{31}H_{21}N_5F_4IrNO_3\cdot0.3CH_2Cl_2$: C 45.9, H 2.7, N 10.3%. Found: C 45.8, H 3.0, N 10.1%.

Characterization Data for ^{H}***Ir•L*^{Me}. ^{1}H NMR (400 MHz, $CDCl_3$): δ 8.30 (1H, d), 8.00 (1H, t), 7.95 (2H, d), 7.90 (1H, d), 7.80 (2H, m), 7.75 (1H, d), 7.70 (1H, d), 7.65 (2H, t), 7.50 (1H, d), 7.29 (1H, d), 7.25 (1H, t), 7.15 (1H, t), 7.04 (2H, m), 6.98 (1H, t), 6.91 (1H, t), 6.87 (1H, t), 6.30 (1H, d), 6.20 (1H, d), 3.35 (3H, s). ES-MS: 660 $(M - NO_3)^+$. Anal. Calc. for $C_{31}H_{25}N_5IrNO_3\cdot0.3CH_2Cl_2$: C 50.3, H 3.5, N 11.2%. Found: C 50.5, H 3.6, N 11.4%.

X-ray Crystallography. Crystals for X-ray diffraction studies were grown from CH_2Cl_2 solutions, either by slow evaporation or by diffusion of hexane vapor into the CH_2Cl_2 solution. In each case a crystal was removed from the mother liquor, coated with oil, and transferred to a stream of cold N_2 on the diffractometer as quickly as possible to prevent decomposition due to solvent loss. All structural determinations were carried out on a Bruker SMART-APEX2 diffractometer using graphite-monochromated Mo−Kα radiation (λ = 0.71073 Å) from a sealed tube source. After integration of the raw data, and before merging, an empirical absorption correction was applied (SADABS)[17] based on comparison of multiple symmetry-equivalent measurements. The structures were solved by direct methods and refined by full-matrix least-squares on weighted F^2 values for all reflections using the SHELX suite of programs.[18] Pertinent crystallographic data are collected in Table 1; selected bond distances (from the metal coordination spheres) are in Table 2.

Flash Photolysis Experiments. Flash photolysis experiments were performed on a home-built setup. The samples were excited at 355 nm with third harmonic of a Q-switched Nd:YAG laser LS-2137U (LOTIS TII). The energy of excitation pulses delivered to the sample was about 2.5 mJ, at 10 Hz repetition rate and 7 ns pulse width. A 150 W Xe arc lamp (Hamamatsu) was used as the probe light source. The probe light was detected through a SPEX MiniMate monochromator by a custom-built detector unit, based on a FEU-118 PMT. Detector current output was coupled into Tektronix TDS 3032B digital oscilloscope and subsequently transferred to the computer. The transient absorption data were corrected for the spontaneous emission from the samples. The same setup was used for the time-resolved emission measurements in the microsecond time domain, with the only difference being a blocked probe lamp. All flash photolysis and microsecond time-resolved emission experiments were performed with the deoxygenated samples, degassed by the freeze−pump−thaw technique, unless noted otherwise. One centimeter path length quartz cells were used.

The analysis of time-resolved data to obtain decay lifetimes was performed using Igor Pro software (WaveMetrics, Inc.) or Origin 8.6 software (OriginLab Co.). The decay kinetics were fitted to the exponential decay law using a least-squares algorithm. Global fitting was applied to analyze simultaneously decay kinetics obtained for numerous spectral points, which enabled us to reconstruct the shape of transient spectra and considerably increased the reliability of the lifetime values.

■ ASSOCIATED CONTENT

Ⓢ Supporting Information

X-ray crystallography data in CIF format. This material is available free of charge via the Internet at http://pubs.acs.org.

■ AUTHOR INFORMATION

Corresponding Author

*E-mail: julia.weinstein@sheffield.ac.uk (J.A.W.), m.d.ward@sheffield.ac.uk (M.D.W.).

Notes

The authors declare no competing financial interest.

■ ACKNOWLEDGMENTS

We thank the EPSRC (UK) and The Leverhulme Trust for financial support.

REFERENCES

(1) Reviews: (a) Ward, M. D. *Coord. Chem. Rev.* **2007**, *251*, 1663. (b) Ward, M. D. *Coord. Chem. Rev.* **2010**, *254*, 2634. (c) Chen, F. F.; Chen, Z.-Q.; Bian, Z.-Q.; Huang, C.-H. *Coord. Chem. Rev.* **2010**, *254*, 991. (d) Faulkner, S.; Natrajan, L. S.; Perry, W. S.; Sykes, D. *Dalton Trans.* **2009**, 3890. (e) Aboshyan-Sorgho, L.; Cantuel, M.; Petoud, S.; Hauser, A.; Piguet, C. *Coord. Chem. Rev.* **2012**, *256*, 1644.

(2) (a) Davies, G. M.; Pope, S. J. A.; Adams, H.; Faulkner, S.; Ward, M. D. *Inorg. Chem.* **2005**, *44*, 4656. (b) Lazarides, T.; Sykes, D.; Faulkner, S.; Barbieri, A.; Ward, M. D. *Chem.—Eur. J.* **2008**, *14*, 9389. (c) Tart, N. M.; Sykes, D.; Sazanovich, I.; Tidmarsh, I. S.; Ward, M. D. *Photochem. Photobiol. Sci.* **2010**, *9*, 886. (d) Sykes, D.; Ward, M. D. *Chem. Commun.* **2011**, *47*, 2279. (e) Sykes, D.; Tidmarsh, I. S.; Barbieri, A.; Sazanovich, I. V.; Weinstein, J. A.; Ward, M. D. *Inorg. Chem.* **2011**, *50*, 11323. (f) Edkins, R. M.; Sykes, D.; Beeby, A.; Ward, M. D. *Chem. Commun.* **2012**, *48*, 9977. (g) Lazarides, T.; Tart, N. M.; Sykes, D.; Faulkner, S.; Barbieri, A.; Ward, M. D. *Dalton Trans.* **2009**, 3971.

(3) (a) Mehlstaubl, M.; Kottas, G. S.; Colella, S.; De Cola, L. *Dalton Trans.* **2008**, 2385. (b) Chen, F.-F.; Bian, Z.-Q.; Lou, B.; Ma, E.; Liu, Z.-W.; Nie, D.-B.; Chen, Z.-Q.; Bian, J.; Chen, Z.-N.; Huang, C.-H. *Dalton Trans.* **2008**, 5577. (c) Chen, F.-F.; Bian, Z.-Q.; Liu, Z.-W.; Nie, D.-B.; Chen, Z.-Q.; Huang, C.-H. *Inorg. Chem.* **2008**, *47*, 2507. (d) Coppo, P.; Duati, M.; Kozhevnikov, V. N.; Hofstraat, J. W.; De Cola, L. *Angew. Chem., Int. Ed.* **2005**, *44*, 1806. (e) Lian, P.; Wei, H.; Zheng, C.; Nie, Y.; Bian, J.; Bian, Z. *Dalton Trans.* **2011**, *40*, 5476. (f) Nonat, A. M.; Allain, C.; Faulkner, S.; Gunnlaugsson, T. *Inorg. Chem.* **2010**, *49*, 8449. (g) Tropiano, M.; Kilah, N. L.; Morten, M.; Rahman, H.; Davis, J. J.; Beer, P. D. *J. Am. Chem. Soc.* **2011**, *133*, 11847. (h) Di Piazza, E.; Norel, L.; Costuas, K.; Bourdolle, A.; Maury, O.; Rigaut, S. *J. Am. Chem. Soc.* **2011**, *133*, 6174. (i) Xie, Z.-L.; Xu, H.-B.; Geβner, A.; Kumke, M. U.; Priebe, M.; Fromm, K.; Taubert, A. *J. Mater. Chem.* **2012**, *22*, 8110. (j) Tropiano, M.; Record, C. J.; Morris, E.; Rai, H. S.; Allain, C.; Faulkner, S. *Organometallics* **2012**, *31*, 5673. (k) Aboshyan-Sorgho, L.; Nozary, H.; Aebischer, A.; Bünzli, J.-C. G.; Morgantini, P.-Y.; Kittilstved, K. R.; Hauser, A.; Eliseeva, S. V.; Petoud, S.; Piguet, C. *J. Am. Chem. Soc.* **2012**, *134*, 12675.

(4) (a) Bünzli, J.-C. G.; Eliseeva, S. V. *J. Rare Earths* **2010**, *28*, 824. (b) Allain, C.; Faulkner, S. *Future Med. Chem.* **2010**, *2*, 339. (c) Bünzli, J.-C. G. *Chem. Rev.* **2010**, *110*, 2729. (d) Pandya, S.; Yu, J.-H.; Parker, D. *Dalton Trans.* **2006**, 2757.

(5) (a) El-ghayoury, A.; Harriman, A.; Ziessel, R. *J. Phys. Chem.* **2000**, *104*, 7906. (b) Benniston, A. C.; Harriman, A. *Coord. Chem. Rev.* **2008**, *252*, 2528.

(6) (a) Flamigni, L.; Barbieri, A.; Sabatini, C.; Ventura, B.; Barigelletti, F. *Top. Curr. Chem.* **2007**, *281*, 143. (b) Chen, Z.-Q.; Bian, Z.-Q.; Huang, C.-H. *Adv. Mater.* **2010**, *22*, 1534. (c) Mydlak, M.; Bizzarri, C.; Hartmann, D.; Sarfert, W.; Schmid, G.; De Cola, L. *Adv. Funct. Mater.* **2010**, *20*, 1812. (d) Orselli, E.; Kottas, G. S.; Konradsson, A. E.; Coppo, P.; Fröhlich, R.; De Cola, L.; van Dijken, A.; Büchel, M.; Börner, H. *Inorg. Chem.* **2007**, *46*, 11082. (e) Sajoto, T.; Djurovich, P. I.; Tamayo, A. B.; Oxgaard, J.; Goddard, W. A.; Thompson, M. E. *J. Am. Chem. Soc.* **2009**, *131*, 9813. (f) He, L.; Duan, L.; Qiao, J.; Wang, R.; Wei, P.; Wang, L.; Qiu, Y. *Adv. Funct. Mater.* **2008**, *18*, 2123. (g) Orselli, E.; Albuquerque, R. Q.; Fransen, P. M.; Fröhlich, R.; Janssen, H. M.; De Cola, L. *J. Mater. Chem.* **2008**, *38*, 4579.

(7) Ward, M. D. *Chem. Commun.* **2009**, 4487.

(8) (a) Stephenson, A.; Ward, M. D. *Dalton Trans.* **2011**, *40*, 7824. (b) Tidmarsh, I. S.; Faust, T. B.; Adams, H.; Harding, L. P.; Russo, L.; Clegg, W.; Ward, M. D. *J. Am. Chem. Soc.* **2008**, *130*, 15167.

(9) (a) Morales, A. F.; Accorsi, G.; Armaroli, N.; Barigelletti, F.; Pope, S. J. A.; Ward, M. D. *Inorg. Chem.* **2002**, *41*, 6711. (b) Ford, W. E.; Rodgers, M. A. J. *J. Phys. Chem.* **1992**, *96*, 2917. (c) Tyson, D. S.; Henbest, K. B.; Bialecki, J.; Castellano, F. N. *J. Phys. Chem. A* **2001**, *105*, 8154. (d) Hissler, M.; Harriman, A.; Khatyr, A.; Ziessel, R. *Chem.—Eur. J.* **1999**, *5*, 3366.

(10) (a) Ferguson, J.; Iredale, T.; Taylor, J. A. *J. Chem. Soc.* **1954**, 3160. (b) Priestley, E. B.; Haug, A. *J. Chem. Phys.* **1968**, *49*, 622. (c) Marchetti, A. P.; Kearns, D. P. *J. Am. Chem. Soc.* **1968**, *89*, 768. (d) Merkel, P. B.; Dinnocenzo, J. P. *J. Photochem. Photobiol. A: Chem.* **2008**, *193*, 110.

(11) (a) Wang, X.; Kofron, W. G.; Kong, S.; Rajesh, C. S.; Modarelli, D. A.; Lim, E. C. *J. Phys. Chem. A* **2000**, *104*, 1461. (b) Dempster, D. N.; Morrow, T.; Quinn, M. F. *J. Photochem.* **1973/4**, *2*, 329. (c) Astier, R.; Meyer, Y. H. *Chem. Phys. Lett.* **1971**, *11*, 523. (d) Hadley, S. G.; Keller, R. A. *J. Phys. Chem.* **1969**, *73*, 4351.

(12) Dakkach, M.; Lopez, M. I.; Romero, I.; Rodriguez, M.; Atlamsani, A.; Parella, T.; Fontrodona, X.; Llobet, A. *Inorg. Chem.* **2010**, *49*, 7072.

(13) (a) Sprouse, S.; King, A. K.; Spellane, P. J.; Watts, R. J. *J. Am. Chem. Soc.* **1984**, *106*, 6647. (b) Coppo, P.; Plummer, E. A.; De Cola, L. *Chem. Commun.* **2004**, 1774. (c) Ragni, R.; Plummer, E. A.; Brunner, K.; Hofstraat, J. W.; Babudri, F.; Farinola, G. M.; Naso, F.; De Cola, L. *J. Mater. Chem.* **2006**, *16*, 1161.

(14) Richards, M. F.; Wagner, W. F.; Sands, D. E. *J. Inorg. Nucl. Chem.* **1968**, *30*, 1275.

(15) Demas, J. N.; Crosby, G. A. *J. Phys. Chem.* **1971**, *75*, 991.

(16) (a) Namdas, E. B.; Ruseckas, A.; Samuel, I. D. W. *J. Phys. Chem. B* **2004**, *108*, 1570. (b) King, K. A.; Spellane, P. J.; Watts, R. J. *J. Am. Chem. Soc.* **1985**, *107*, 1431.

(17) Sheldrick, G. M. *SADABS: A program for absorption correction with the Siemens SMART system*; University of Göttingen: Göttingen, Germany, 1996.

(18) Sheldrick, G. M. *Acta Crystallogr., Sect. A* **2008**, *64*, 112.